Proceedings of IMECE2008
2008 ASME International Mechanical Engineering Congress and Exposition
October 31-November 6, 2008, Boston, Massachusetts, USA

IMECE2008-67273

PLANAR ROBOTIC SYSTEMS FOR UPPER-LIMB POST-STROKE REHABILITATION

Giulio Rosati*, Riccardo Secoli, Damiano Zanotto, Aldo Rossi
Dept. of Innovation in Mechanics and Management (DIMEG)
University of Padua - Faculty of Engineering
via Venezia 1, 35131 Padova, Italy
giulio.rosati@unipd.it

Giovanni Boschetti
Dept. of Management and Engineering (DTG)
University of Padua - Faculty of Engineering
Stradella S. Nicola 6, 36100 Vicenza, Italy
giovanni.boschetti@unipd.it

ABSTRACT

Rehabilitation is the only way to promote recovery of lost function in post-stroke hemiplegic subjects, leading to independence and early reintegration into social and domestic life. In particular, upper limb rehabilitation is fundamental to regain ability in Activities of Daily Living (ADLs). Robot-aided rehabilitation is an emerging field seeking to employ leading-edge robotic systems to increase patient recovery in the rehabilitation treatment. Even though the effectiveness of robotic therapy is still being discussed, the use of robotic devices can increase therapists' efficiency by alleviating the labor-intensive aspects of physical rehabilitation, and can produce a reduction in treatment costs.

This paper presents a comparison between different planar robotic devices designed for upper-limb rehabilitation in chronic patients. A planar configuration of the workspace leads to straightforward mechanical and control system design, and allows to define very simple and understandable treatment exercises. Also, the graphical user interface becomes very intuitive for the patient, and a set of Cartesian-based measures of the patient's performance can be defined easily.

In the paper, SCARA [1] robots such as the MIT-Manus, Cartesian robots and cable-driven robots are considered and compared in terms of inertial properties and force exertion capabilities. Two cable-driven devices, designed at the Robotics Lab of the Department if Innovation In Mechanics and Management, University of Padua, Italy, are presented for the first time. The first robot employs four driven cables to produce a planar force on the end-effector, whereas the second one is based on a three-cable configuration plus a linear actuator to obtain better overall robot performance.

INTRODUCTION

Recent research in Europe and in the U.S. show that brain injury is one of the most increasing health diseases of the last decade [1, 2]. Only in the U.S. there are 700,000 new cases each year [3] while in Europe there are 200 to 300 new stroke cases per 100,000 every year [4]. This is alarming when viewed in terms of current U.S. and Europe demographic trends, which show that individuals over 65 years are the fastest growing segment of our population [5]. In conjunction, the public health cost increase causes many rehabilitation centers to provide low therapist-to-patient ratios, with heavy reliance on outpatient rehabilitation [2]. These treatment philosophy is in contrast with recent reports suggesting that recovery of post-stroke patients is maximized in the first days after injury, when patients receive one-on-one, repetitive therapy. Many post-stroke survivors are affected by upper and lower limb hemi-paresis causing an incorrect behavior: the patient usually tends to overuse the less-affected limb and under-use the impaired limb. Repetitive practice of skilled tasks are thought to be particularly beneficial to stroke survivors due to the fact that they cause neurological-remapping and brain plasticity [6, 7].

These are the key issues that encouraged the development of robotic devices for rehabilitation therapy in the recent past [8]. The rehabilitation goal is to promote recovery of lost function, leading to independence and early reintegration into social

*Address all correspondence related to this paper to this author.
[1]Selective Compliance Assembly Robot Arm

and domestic life. The use of robotic devices in rehabilitation can provide high-intensity, task-specific upper limb treatment, consisting of passive, active-assistive or active highly repetitive movements. Another important goal of post-stroke rehabilitation is the conservation and progressive increase of motor-capability. To achieve this aim, it is necessary to continue the treatment after hospital discharge with constant medical care. Technology can now permit the delivery of robot-aided neurological rehabilitation treatment in a safe, reliable, effective manner. A limited number of clinical trials has been conducted so far, with positive but modest results for chronic patients [9, 10]. There is some evidence that better results may be obtained in the sub-acute phase [11, 12], but this point needs to be further investigated in the next future.

Several mechatronic systems have been developed to achieve the recovery of the upper limb function. Two different types of devices can be defined. The first are the Exoskeleton-like machines, which are wearable bio-mechatronic systems that follow the patient's limb movement. This type of machine is very complex because the therapy exercise can be directly defined in patient joint space and a separate control for different joints should be implemented in order to restore the natural motor control strategies. The second type are the Operational Machines, in which the contact between the patient and the therapy device is obtained only at the end-effector of the robot. The therapy exercise is programmed in the Cartesian space or in the robot joint space, and the patient interacts with the robot following a trajectory in the operational space. The aim of this paper is to compare, from a mechanical point of view, different examples of the second type of machines. In particular, the planar devices designed for the treatment of chronic patients will be investigated.

PLANAR ROBOTIC SYSTEMS FOR REHABILITATION

There are many good reasons to choose a planar workspace (WSP) for a rehabilitation robot. First of all, the planar configuration leads to straightforward mechanical and control system design, and allows to define very simple and understandable treatment exercises. Also, the graphical user interface becomes very intuitive for the patient. Finally, a set of Cartesian-based measures of the patient's performance can be defined easily, to obtain a score for the exercise and a measure of patient involvement in the rehabilitation treatment. The main drawback of this choice is probably that the patient's shoulder is not trained as much as in 3D exercises, and this may lead to lower gains in patient recovery. This problem can be partially overcome by tilting the workspace of the robot.

Planar haptic devices for upper limb rehabilitation can be classified into three main groups: SCARA robots, Cartesian robots and wire-based robots. Several different prototypes have been developed so far; for the purpose of this work, four different devices will be analyzed.

SCARA devices

The most famous example of planar rehabilitation robot is the MIT/Manus [13, 14] whose first prototype was made in the early nineties at the Massachusetts Institute of Technology. The mechanical structure of this robot is composed of a direct-drive five bar-linkage SCARA mechanism, that provides two translational degrees of freedom in a planar workspace. The Human Machine Interface of MIT/Manus consists in an LCD panel located in front of the patient, where the therapy exercise is represented. A sample exercise consists in moving a colored circle (the End Effector) to a target position inside the workspace. The commercial version of the MIT-Manus is the InMotion^{TM}by Interactive Motion Technologies, Inc. (Cambridge, MA). A similar prototype, named Braccio di Ferro [15], was built in the Neurolab of the Department of Informatics, Systems and Telecommunications at University of Genova, Italy. This device is very similar to the MIT-Manus, but there are some differences in mechanical design (the ability to tilt the planar workspace), motor power (steady hand forces are nearly three times greater), and virtual environment (Simulink-based).

Cartesian devices

Another way to obtain a planar workspace is to employ Cartesian devices. The first prototype of such a device for rehabilitation is named MEMOS [16, 17] and is currently undergoing clinical trials at Fondazione S. Maugeri, Veruno (NO), Italy. One recent evolution of this device is the CBM-Motus [18] which was developed at the Biomedical Robotics and EMC Laboratory, University Campus Bio-Medico, Rome, Italy. The kinematic structure of the CBM-motus is based on two identical square modules connected by a double prismatic joint. Each module consists in six pulleys (all with the same radius) and two toothed belts. Workspace vertexes are the pulleys themselves, and the boundary is formed by the belts linked to the pulleys. Inside the workspace, that is $500mm \times 500mm$ in size, there are two bars. Each bar is connected to a module that allows the motion in a single direction (x and y). The bars slide through a compound prismatic joint to which the end-effector is connected. Belt's motion is controlled by two DC brushless motors. The mechanical design was built up to achieve high back-drivability, a large workspace and a minimum interaction force of $50N$. The HMI is similar to those of the MIT-Manus.

Cable-driven devices

A planar workspace can be easily obtained with cable-driven devices. Two examples of such robots for neurorehabilitation are the Sophia-3 and the Sophia-4, developed by the Mechatronics Team at the Dept. of Innovation in Mechanics and Management (DIMEG), University of Padua, Italy. The first rehabilitation robots designed at DIMEG are the NeRebot [19] and the Maribot [20]. These cable-suspended robots have a 3D workspace

and were designed to join the standard rehabilitation therapy in the sub-acute phase. On the contrary, the planar devices were tailored to the rehabilitation treatment of chronic patients.

The mechanical design of Sophia-4 (*String Operated Planar Haptic Interface for upper-Arm rehabilitation*) derives from a previous prototype named the FeRiBa3 [21], a general-purpose table-top haptic display. Fig. 1 shows the schematic layout of Sophia-4. The machine is made up of a planar surface on which the end-effector can be moved. The aluminum hand-bar grip (end-effector) has two degrees of freedom. The force on the end-effector is obtained by stretching four nylon cables by means of DC motors. One end of each cable is fixed to the center of the grip, the other end is directly keyed to a direct-drive pulley after passing through an entry point. The entry-points are designed to spin around a vertical axis to maintain constant cable lengths unless the end-effector is driven in the direction of the entry point.

The trapezoidal workspace was shaped to favor patient movements during robot therapy, avoiding collisions with the cables. The dimensions of the workspace were calculated considering the dimensions of patient's body [22], the distance between the trunk of the patient and the haptic device, and the maximum isotropic force to be exerted in the workspace. The workspace can be easily re-drawn by simply changing the disposition of the four entry-points on the planar surface. In this case, the control system needs only to be taught with the new coordinates of the entry-point positions.

The second planar rehabilitation device is the Sophia-3, that came up as an evolution of Sophia-4. Mechanical design was reviewed to achieve better performance indexes in the whole workspace and to reduce the risk of cable-patient interference. As shown in Fig. 2 the basement structure is similar to the one of Sophia-4. The main difference consists in using a moving motor-pulley block to substitute the two motors close to the patient. Workspace size remains unchanged, while human-cable interference is drastically reduced. The Sophia-3 employs four DC motors, three directly linked to the cables and one used to

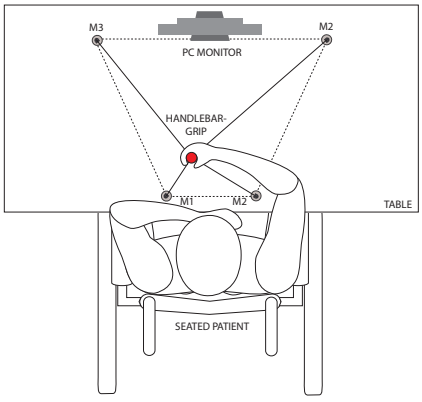

Figure 1. SOPHIA-4 TOP VIEW.

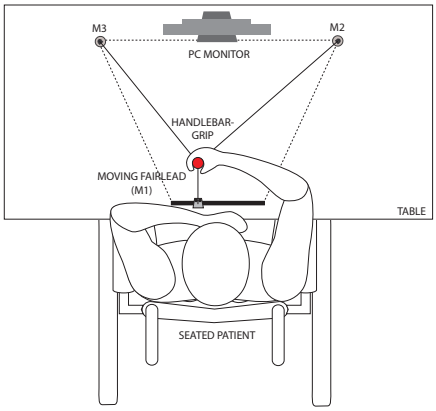

Figure 2. SOPHIA-3 TOP VIEW.

control the moving motor-pulley block, which carries the motor of the moving cable. The entry point of this cable is moved in such a way that the cable itself remains always orthogonal to the translation axis [23].

PERFORMANCE EVALUATION

With the aim of comparing these different designs of planar robots, several performance indexes have been considered, which are typically applied to the design of industrial manipulators. Examples of such parameters can be easily found in the literature, as they are often utilized in combination to construct a cost function to be minimized in the design optimization problem. A basic classification separates kinetostatic indexes from the dynamic ones. Several parameters are specifically tailored to non-redundant manipulators, and hence cannot be applied to parallel robots or wire-based system with redundant actuation.

Kinetostatic parameters based on the pseudo-inverse of the Jacobian matrix are often used to evaluate the performances of a manipulator. By mapping through this matrix the unit hypersphere of joint velocities into the operational-space, the *velocity manipulability ellipsoid* is derived: it expresses the ease of arbitrarily changing the position and orientation of the end-effector in a given configuration. A manipulability measure has been introduced (Yoshikawa, [24]) which is proportional to the volume of the ellipsoid, while a measure of the kinematic isotropy of the mechanism has been derived form the inverse of the Jacobian condition number. Thanks to the velocity-force duality, another ellipsoid, called the *force manipulability ellipsoid*, can be derived. The principal axes are the same of the previous ellipsoid, while their lengths are the reciprocal of the previous ones.

Unfortunately, this duality does not hold for parallel manipulators with actuation redundancy (PMAR): this is also the case of cable-driven manipulators. For those manipulators, S. Krut et al. proved how the velocity ellipsoid is no longer the feasible ellipsoid having the maximum area, and the Jacobian condition

number does not reflect kinematic isotropy. Different indexes are presented, based on the (actual) ellipsoid with maximum area belonging to the operational velocity polytope [25]. Similarly, force exertion capabilities cannot rely on the Jacobian condition number: more appropriate indexes can be derived from the operational force polytope. In [26], for instance, the same authors suggested the use of the maximum feasible isotropic operational force. Actually, the maximum isotropic force had already been adopted as a manipulability index for wire-based robots in a previous work by P. Gallina, G. Rosati et al. [21].

As far as mass properties and dynamic behavior of manipulators are concerned, two aspects have to be investigated at least: inertial properties and acceleration performances of the end-effector. The *Generalized Inertia Ellipsoid* (GIE) approach was first introduced by H. Asada [27] for the design of serial manipulators with only translating end-effector (EE). The GIE is derived from the quadratic form associated with the task-space kinetic energy matrix, and represents the extension of the inertia ellipsoid of a single rigid body to a series of rigid bodies. By drawing a vector connecting the center of the ellipsoid to a point on its boundary and taking the inverse of its square root, a measure proportional to the generalized moment of inertia along the same direction is obtained: thus the maximum moment of inertia is to be expected along the minor axis of the ellipsoid. Since the GIE varies depending on the pose of the end-effector, the generalized moment of inertia depends also on the configuration of the manipulator. From the observation of the task-space equation of motion it is clear that inertial properties depend also on Coriolis and centrifugal non-linear contributions. Those contributions arise from the changes of the inertial tensor with configuration: thus, if the changes in shape and orientation of the GIE are considerable over the working space, large nonlinear forces have to be expected, conversely, if the GIE is isotropic, such forces are not present.

For a generic manipulator with both translational and rotational degrees of freedom, the previous analysis would result in a poorly significant mixture of mass and inertial properties. To overcome this issues, O. Khatib [28] proposed a decomposition of the task-space kinetic energy matrix into three submatrices.

Yoshikawa et al. [29] introduced the *Dynamic Manipulability Ellipsoid* (DME), which is a common tool to determine the ability of a manipulator to produce arbitrary acceleration when the arm is staying still, for a given set of torques at joints.

Clearly, the most desirable acceleration capabilities are those isotropic and uniform over the whole workspace. O. Khatib and A. Bowling developed a method to investigate the acceleration capabilities of manipulators, called the *ellipsoid expansion model.* This approach allows to evaluate how joint torque constraints affect end-effector isotropic linear and angular accelerations and velocities [30–32]. The acceleration performance measures derived from these results have been used inside a cost function for an optimization procedure.

Selected indexes

Starting from the previous considerations, the maximum isotropic force i_F, the GIE euclidean norm $\|\mathbf{\Lambda}\|$ and the condition number $\kappa(\mathbf{\Lambda})$ have been selected. These performance indexes have been used to compare the following robots: MIT-Manus (SCARA type), CBM-Motus (Cartesian type), Sophia-3 and Sophia-4 (wire-based type).

The maximum isotropic force has been chosen to assess the kinetostatic performances. Its value can be very useful for the control of such robotic systems, since the forces the patient will exert during the therapy cannot be determined in advance. In addition, this parameter can be easily computed both for robots with rigid links and for wire-based ones.

As far as inertial capabilities are concerned, the GIE euclidean norm and condition number are used as performance parameters. This is mainly due to the effect of the end-effector inertial properties on the *haptic transparency* of the system (i.e. the fidelity with which virtual object properties are presented to, and perceived by the human operator [33]). Robotic systems utilized in rehabilitation are essentially haptic devices, since they interface the patient to a virtual environment (i.e. the rehabilitation game) via the sense of touch, by applying forces and/or motions to the user. Clearly, the ideal haptic interface should be perfectly transparent, which implies the constant equivalence between transmitted impedance and task impedance. In particular, for rehabilitation robots, a large transparency is desirable to allow a better transmission of assistive forces. Moreover, a further improvement has to be expected when the robotic assistance is not required: since the patient perceives a little impedance, the tasks are accomplished just as if the arm were free to move in the working space.

Haptic transparency depends both on the dynamic properties of the mechanical system and on the control architecture. The former, in turn, depends on inertial characteristics and acceleration performances. For a given configuration, the maximum actuation torques restrict the set of allowable end-effector velocities and accelerations. However, for our application, this aspect is negligible. Conversely, the isotropy of the end-effector inertial properties (i.e., $\kappa(\mathbf{\Lambda}) = 1$) is a primary concern for robots that interact with humans, as the same inertial impedance should be felt in every direction. Thus, by analyzing the inertial tensor, greater relevance has been imputed to inertial properties, while low operational velocities justify the neglection of non-linear Coriolis and centrifugal terms.

COMPARISON OF INERTIAL PROPERTIES

MIT-Manus

The dynamics of MIT-Manus has been derived by first dividing its mechanical structure into two serial mechanism: the first semi-manipulator controls orientation of link l_{1A} through motor 1, while the orientation of link l_{2B} is indirectly controlled through

motor 2, connected to link l_{2A}, both motors are located at the base of the robot (Fig. 3). Friction is neglected and the infinitely rigid links are assumed . The Newton-Euler equations have been written for each semi-manipulator and successively combined to obtain the dynamic model in the joint space:

$$\begin{aligned}
&\tau = \mathbf{D}_{MIT}(\boldsymbol{\phi})\ddot{\boldsymbol{\phi}} + \mathbf{C}_{MIT}(\boldsymbol{\phi},\dot{\boldsymbol{\phi}})\dot{\boldsymbol{\phi}} \\
&\mathbf{D}_{MIT} = \begin{bmatrix} k_{r1} & k_{r3}\cos(\phi_2-\phi_1) \\ k_{r3}\cos(\phi_2-\phi_1) & k_{r2} \end{bmatrix} \\
&\mathbf{C}_{MIT} = \begin{bmatrix} 0 & -k_{r3}\sin(\phi_2-\phi_1)\dot{\phi}_2 \\ k_{r3}\sin(\phi_2-\phi_1)\dot{\phi}_1 & 0 \end{bmatrix}
\end{aligned} \tag{1}$$

where $\mathbf{k} = \begin{bmatrix} k_{r1} & k_{r2} & k_{r3} \end{bmatrix}'$ is a vector of constant parameters, given by:

$$\begin{aligned}
&k_{r1} = I_{G1A} + I_{G1B} + d_{1A}^2 m_{1A} + d_{1B}^2 m_{1B} + l_{1A}^2 (m_{2B} + m_{EE}); \\
&k_{r2} = I_{G2A} + I_{G2B} + d_{2A}^2 m_{2A} + d_{2B}^2 m_{2B} + l_{2B}^2 m_{EE} + \\
&+ l_{2A}^2 (m_{1A} + m_{2B} + m_{EE}) - 2 l_{2A} (d_{2B} m_{2B} + l_{2B} m_{EE}); \\
&k_{r3} = -d_{1A} l_{2A} m_{1A} + \\
&- l_{1A} (-d_{2B} m_{2B} - l_{2B} m_{EE} + l_{2A} (m_{2B} + m_{EE}));
\end{aligned} \tag{2}$$

Estimations of the useful link lengths l_{1A}, $(l_{2B} - l_{2A})$ and of vector $\mathbf{k}$ can be found in [34]: $l_{1A} = 0.46$m, $(l_{2B} - l_{2A}) = 0.44$m, $\mathbf{k} = \begin{bmatrix} 0.3189 & 0.0938 & 0.1262 \end{bmatrix}'$. Matrix $\boldsymbol{D}_{MIT}$ is the joint-space kinetic energy matrix. The task-space kinetic matrix $\boldsymbol{\Lambda}_{MIT}$ is obtained from $\boldsymbol{D}_{MIT}$ and the Jacobian matrix $\boldsymbol{J}_{MIT}$:

$$\begin{aligned}
&\boldsymbol{\Lambda}_{MIT} = \mathbf{J}_{MIT}^{-T} \mathbf{D}_{\mathbf{r}} \mathbf{J}_{MIT}^{-1} \\
&\mathbf{J}_{MIT} = \begin{bmatrix} -l_{1A}\sin\varphi_1 & -(l_{2B}-l_{2A})\sin\varphi_2 \\ l_{1A}\cos\varphi_1 & (l_{2B}-l_{2A})\cos\varphi_2 \end{bmatrix}
\end{aligned} \tag{3}$$

CBM-Motus

Following the dynamic model presented in [18], CBM-Motus has been treated as a Cartesian robot with two prismatic joints d_1 and d_2. Thus, the Jacobian matrix is trivial, and derivation of $\boldsymbol{\Lambda}_{CBM}$ is straigthforward:

$$\begin{aligned}
&\mathbf{D}_{CBM} = \begin{bmatrix} m_{l1} + I_{m1}/R^2 & 0 \\ 0 & m_{l2} + I_{m2}/R^2 \end{bmatrix} \\
&\mathbf{J}_{CBM} = \mathbf{I_2} \\
&\boldsymbol{\Lambda}_{CBM} = \mathbf{J}_{CBM}^{-T} \mathbf{D}_{CBM} \mathbf{J}_{CBM}^{-1} = \mathbf{D}_{CBM}
\end{aligned} \tag{4}$$

where m_{l1} and I_{m1} are the total translating mass the total moment of inertia pertaining to each degree of freedom and $R = 25$mm is the radius of the pulleys. The estimated values for the diagonal components of the mass matrix are: $\boldsymbol{\Lambda}_{CBM,(1,1)} = \boldsymbol{\Lambda}_{CBM,(2,2)} = 2.59$kg.

Sophia-3 and Sophia-4

The dynamic models for Sophia-3 and Sophia-4 have been derived by using the *force-closure equation* to combine the Cartesian dynamic model of the end-effector with the dynamics equations of the actuators subsystems [35]. The torque required to turn the i-th pulley shaft is:

$$\tau_i = f_i r_{pi} + I_{pi} \frac{\ddot{\theta}_{mi}}{k_{ri}} + b_i \frac{\dot{\theta}_{mi}}{k_{ri}} \tag{5}$$

and the torque required at the i-th motor shaft is:

$$\tau_{mi} = \frac{\tau_i}{k_{ri}} + I_{mi}\ddot{\theta}_{mi} + b_{mi}\dot{\theta}_{mi} \tag{6}$$

where f_i is the i-th cable tension, r_{pi} is the i-th pulley radius, k_{ri} the reduction ratio of the i-th gearbox. I_{pi} and I_{mi} are the moment of inertia of the i-th pulley and of the i-th motor respectively, while b_i and b_{mi} are the viscous damping coefficients. By substituting Eqn. 5 into Eqn. 6, and solving for f_i, the following expression is obtained for the i-th cable tension:

$$f_i = -\left(I_{mi}\frac{k_{ri}}{r_{pi}} + \frac{I_i}{k_i}\right)\ddot{\theta}_{mi} - \left(b_{mi}\frac{k_{ri}}{r_{pi}} + \frac{b_i}{k_i}\right)\dot{\theta}_{mi} + \frac{k_{ri}}{r_{pi}}\tau_{mi} \tag{7}$$

Now, using the reverse kinematics formulas, each θ_{mi} can be expressed as a function of the end-effector position $\mathbf{x}$:

$$\theta_{mi} = \frac{k_{ri}}{r_{pi}}\left(L_{0i} + d(\mathbf{x}, \mathbf{x}_{mi})\right) \tag{8}$$

where L_{0i} is the length of cable i when the end-effector lays in the origin of the reference frame. By successively taking the

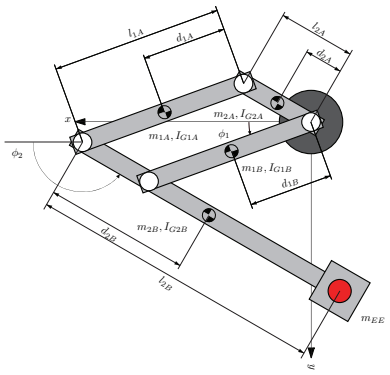

Figure 3. MIT-MANUS SCHEMATIC TOP VIEW.

r_{pi}[mm]	23	J_{mi}[kgm^2]	3.0e-5
k_{ri}	1	J_{pi}[kgm^2]	15.75e-6
m_{EE}[kg]	0.5	M_0[N]	2

Table 1. SOPHIA-3 AND SOPHIA-4 MODEL PARAMETERS.

time derivative of Eqn. 8, expressions for $\dot{\theta}_{mi}$ and $\ddot{\theta}_{mi}$ are derived. These expressions can be substituted into Eqn. 7, and all the components can be combined in a single vectorial expression:

$$\mathbf{f} = -\mathbf{J}\left(\frac{\partial \boldsymbol{\theta_m}}{\partial \mathbf{x}}\ddot{\mathbf{x}} + \frac{d}{dt}\frac{\partial \boldsymbol{\theta_m}}{\partial \mathbf{x}}\dot{\mathbf{x}}\right) - \mathbf{B}\frac{\partial \boldsymbol{\theta_m}}{\partial \mathbf{x}}\dot{\mathbf{x}} + \mathbf{K}_r\boldsymbol{\tau}_m \qquad (9)$$

where $\boldsymbol{J}$, $\boldsymbol{B}$ and $\boldsymbol{K}_r$ are diagonal matrices, containing the constant parameters of Eqn. 7. Since cables can only pull, Eqn. 9 holds as long as each component of $\mathbf{f}$ is non-negative. However, we can take advantage of actuation redundancy and choose appropriate $\boldsymbol{\tau}_m$, so that cable tension are always maintained above a given minimum value $f_{\min}$. The Cartesian dynamic equations for the point-mass end-effector are given by:

$$\mathbf{F} = m_{EE}\ddot{\mathbf{x}} \qquad (10)$$

If the right-hand sides of Eqn. 10 and Eqn. 9 are substituted into the force-closure equation ($\mathbf{F} = \mathbf{A}(\mathbf{x})\mathbf{f}$), the Cartesian dynamic equations of the system are derived:

$$\boldsymbol{\Lambda}(\mathbf{x})\ddot{\mathbf{x}} + \mathbf{N}(\dot{\mathbf{x}},\mathbf{x}) = \mathbf{A}(\mathbf{x})\mathbf{K}_r\boldsymbol{\tau_m} \qquad (11)$$

where $\mathbf{A}(\mathbf{x})$ is the configuration-dependent *structure matrix*, $\boldsymbol{\Lambda}(\mathbf{x})$ is the mass matrix and $\mathbf{N}(\dot{\mathbf{x}},\mathbf{x})$ the vector of centrifugal and friction contributes:

$$\begin{aligned}
&\mathbf{A}(\mathbf{x}) = \begin{bmatrix}\mathbf{v}_1 \ \ldots \ \mathbf{v}_m\end{bmatrix}' \\
&\boldsymbol{\Lambda}(\mathbf{x}) = m_{EE}\mathbf{I}_2 + \mathbf{A}(\mathbf{x})\mathbf{J}\frac{\partial \boldsymbol{\theta_m}}{\partial \mathbf{x}} \\
&\mathbf{N}(\dot{\mathbf{x}},\mathbf{x}) = \mathbf{A}(\mathbf{x})\left(\mathbf{J}\frac{d}{dt}\frac{\partial \boldsymbol{\theta_m}}{\partial \mathbf{x}}\dot{\mathbf{x}} + \mathbf{B}\frac{\partial \boldsymbol{\theta_m}}{\partial \mathbf{x}}\dot{\mathbf{x}}\right)
\end{aligned} \qquad (12)$$

$\boldsymbol{v_i}$ is the unit vector directed along the *i*-th cable, pointing toward the corresponding ground link connection point.
In order to compute $\boldsymbol{\Lambda}(\mathbf{x})$ for Sophia-4 and Sophia-3, the values in Tab. 1 have been used.

Results

Figures 4 and Fig. 5 respectively illustrate the values of $\|\boldsymbol{\Lambda}_{MIT}\|$ and $\kappa(\boldsymbol{\Lambda}_{MIT})$ throughout the workspace of the MIT-Manus. The workspace area has been estimated assuming that

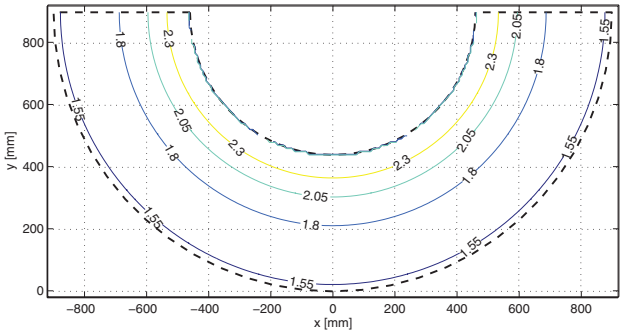

Figure 4. $\|\boldsymbol{\Lambda}_{MIT}\|$[kg], MAXIMUM MASS PERCEIVED AT THE END-EFFECTOR OF THE MIT-MANUS THROUGHOUT THE WORKSPACE.

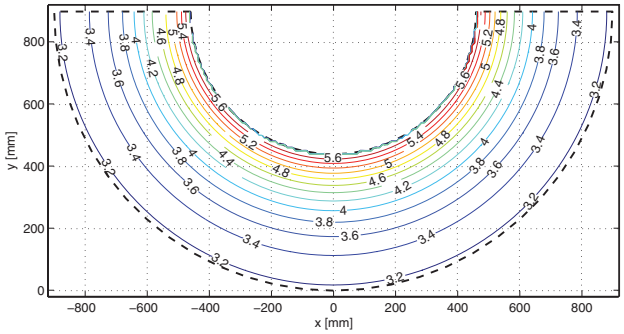

Figure 5. ISOTROPICITY OF THE INERTIAL PROPERTIES OF THE MIT-MANUS: $\kappa(\boldsymbol{\Lambda}_{MIT})$ RATIO BETWEEN THE MAXIMUM AND THE MINIMUM MASSES PERCEIVED AT THE END EFFECTOR.

$\varphi_1 \in [0;\pi]$ and $(\varphi_2 - \varphi_1) \in [0;\pi/2]$. The contour lines have a semicircular shape and show more favorable values near the patient (bottom side of the workspace). The perceived mass is always greater than 1.5kg. When motors are idle and the robot is driven by external forces applied at the end-effector, movements that do not require variations of the elbow joint are much easier, the gap between radial and tangential movements becoming more pronounced near the base of the device. Thus, the robot inertial properties are quite anisotropic.

As far as CBM-Motus is concerned, $\boldsymbol{\Lambda}_{CBM}$ is diagonal and independent of end-effector location, so that $\|\boldsymbol{\Lambda}_{CBM}\| = 2.59$kg within the entire workspace (a square having a side $l = 550$mm). Furthermore, since the mass-matrix is a scalar matrix, the robot is isotropic (i.e. the same mass is perceived at the end-effector in every direction) and $\kappa(\boldsymbol{\Lambda}_{CBM}) = 1$.

Figure 6 and Fig. 7 show $\|\boldsymbol{\Lambda}_{S-4}\|$ and $\kappa(\boldsymbol{\Lambda}_{S-4})$: the dynamics of the end-effector is slightly influenced by the presence of the pulleys, since the eccentricity of the GIE is lower than 1.3 and the perceived mass is lower than $1.5m_{EE}$ inside the most part of the workspace. The inertial properties of Sophia-3, represented in Fig. 8 and Fig. 9, show improved results both in terms

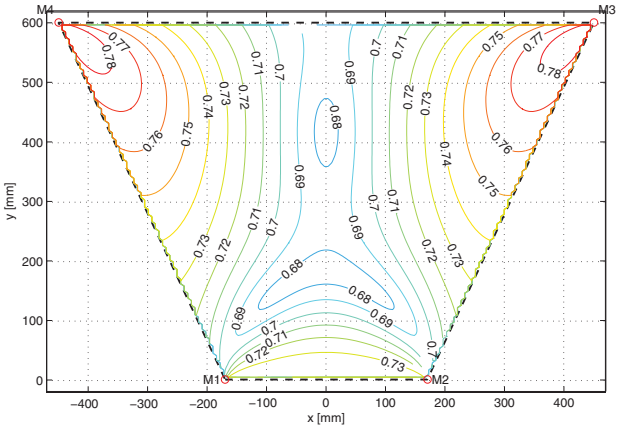

Figure 6. $\|\mathbf{\Lambda}_{S-4}\|$[kg], MAXIMUM MASS PERCEIVED AT THE END-EFFECTOR OF SOPHIA-4.

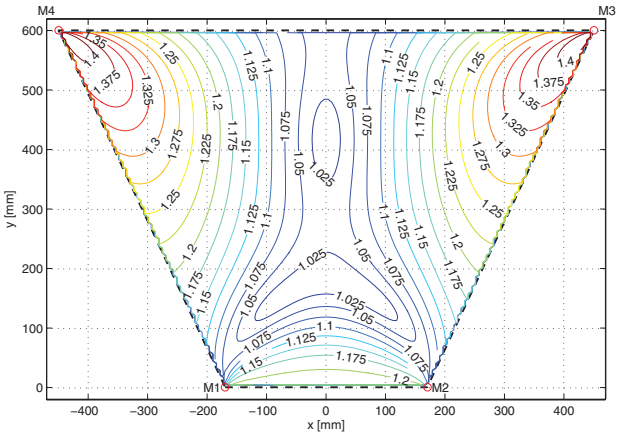

Figure 7. $\kappa(\mathbf{\Lambda}_{S-4})$, ISOTROPICITY OF THE INERTIAL PROPERTIES OF SOPHIA-4.

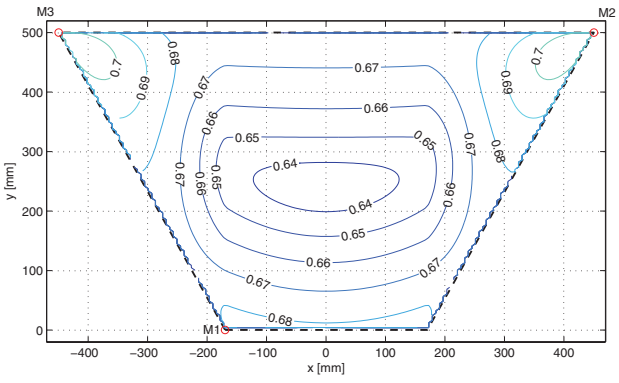

Figure 8. $\|\mathbf{\Lambda}_{S-3}\|$[kg], MAXIMUM MASS PERCEIVED AT THE END-EFFECTOR OF SOPHIA-3.

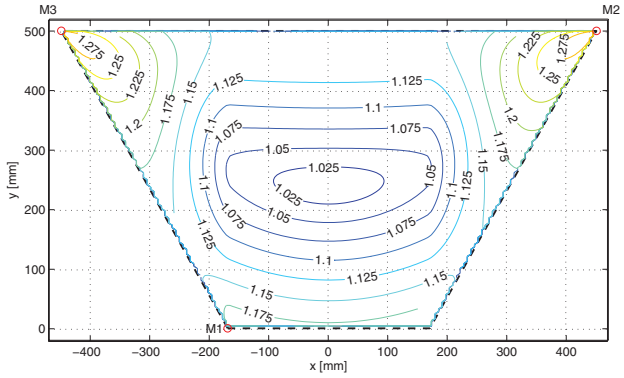

Figure 9. $\kappa(\mathbf{\Lambda}_{S-3})$, ISOTROPICITY OF THE INERTIAL PROPERTIES OF SOPHIA-3.

of maximum perceived mass and in terms of inertial isotropy, being $\|\mathbf{\Lambda}_{S-4}\| < 1.35 m_{EE}$ and $e < 1.2$ in a significant region of the workspace.

Hence, the Cartesian device shows better results than the SCARA robot in terms of inertial isotropy. Nonetheless, the latter presents a lower perceived mass. The wire-based robots give the lowest perceived masses, while keeping an almost isotropic behaviour. Furthermore, if a reference area of the workspace is considered, the level of anisotropy and the maximum perceived mass are approximately constant (Tab. 2).

COMPARISON OF FORCE EXERTION CAPABILITIES

To assess force capabilities, the value of the maximum isotropic force i_F must be computed over the workspace of each robot. In general, two methods can be used to compute the maximum isotropic force of a *n*-DOF manipulator driven by *m* actuated joints. The first one consists in mapping the *m*-dimensional hypercube representing the allowable joint torques into the operational force space, thus obtaining the *n*-dimensional set of forces that can be exerted at the end-effector. The radius of the largest hypersphere contained inside this set gives i_F. On the other hand, one can think of mapping the the *n*-dimensional hypersphere into the joint space, and expanding the resulting set until it reaches the boundaries of the hypercube. While both methods can be applied to non-redundant manipulators, only the first one applies to parallel cable-driven robots.

MIT-Manus

For the MIT-Manus $n = m = 2$, hence the hypersphere reduces to a circle whose equation is: $\boldsymbol{F}^T\boldsymbol{F} = a^2$. As long as the robot does not lay in a singular configuration, the Jacobian matrix $\boldsymbol{J}$ is full rank: thus, by inverting the equation of kinetostatics $\boldsymbol{\tau} = \boldsymbol{J}^T\boldsymbol{F}$ and substituting for $\mathbf{F}$ inside the previous expression,

the equation of the joint-space ellipse is derived:

$$\tau^T \mathbf{K} \tau = a^2 \tag{13}$$

where $\mathbf{K} = \left(\mathbf{J}^T \mathbf{J}\right)^{-1}$. Since $m = 2$, the set of allowable joint torques is a rectangle, centered in the origin of the axes τ_1, τ_2, with vertexes in $(\pm\tau_{1\max}, \pm\tau_{2\max})$. The maximum isotropic force is the maximum value of a that corresponds to a joint-space ellipse entirely contained inside the rectangle. Thus, considering the symmetries, only two values of a must be checked, which correspond to the conditions of tangency with two adjacent sides of the rectangle:

$$\begin{aligned} a_1 &= \tau_{\max 1}\sqrt{K_{11} - \frac{K_{12}^2}{K_{22}}} = \frac{\tau_{\max 1}}{l_{1A}} \\ a_2 &= \tau_{\max 2}\sqrt{K_{22} - \frac{K_{12}^2}{K_{11}}} = \frac{\tau_{\max 2}}{(l_{2B} - l_{2A})} \\ i_F &= \min(a_1, a_2) \end{aligned} \tag{14}$$

Hence, for this manipulator, i_F is configuration independent. Since $l_{1A} > (l_{2B} - l_{2A})$, and the continuous stall torques are $\tau_{\max 1} = \tau_{\max 2} = 7.86$Nm [36]:

$$i_{F,MIT} = \frac{\tau_{\max 1}}{l_{1A}} = \frac{7.86}{0.46} = 17.86N \tag{15}$$

CBM-Motus

The same approach can be applied to the CBM-Motus. According to the model introduced in [18], the two degrees of freedom can be treated as two equivalent prismatic joints, each with a maximum allowable force equal to the ratio of the motor rated torque and the pulley radius, hence: $\mathbf{F}_{\max} = \mathbf{M}/R = 2/0.025 = 80$N. The equivalent joint forces coincide with the operational forces, since the latter are obtained from the former through a trivial mapping ($\mathbf{J} = \mathbf{I_2}$). As a consequence, $i_{F,CBM}$ is the radius of the largest circumference centered in the origin of the axes and included inside a square with $l = 80$N:

$$i_{F,CBM} = 80N \tag{16}$$

Sophia-3 and Sophia-4

When actuation redundancy is involved, the previous approach cannot be applied. Now m is the number of cables and n is the number of degrees of freedom of the end-effector. Each cable tension is constrained by an upper and a lower bound: $f_i \in [f_{i,\min}, f_{i,\max}]$, the former required to keep the cables stretched, the latter due to motors rated torques. Therefore, the m-dimensional joint-space cuboid is defined by $f_{i,\min}$ $f_{i,\max}$, and in order to compute $i_{F,S-4}$ and $i_{F,S-3}$, it must be mapped into the n-dimensional operational space through the structure matrix $\mathbf{A} = \mathbf{J}^{-\mathbf{T}}$. A convex polytope is obtained in the operational space: since $n = 2$, it is actually a polygon, whose vertexes are derived by calculating the *convex hull* of the transformed cuboid vertexes. The radius of the largest circumference is derived by calculating the minimum among the distances of each side of the polytope from the origin.

For Sophia-3 and Sophia-4, pulleys with $r_p = 23$mm are keyed on the shafts of m identical brushless motors, each rated to 2Nm of maximum continuous torque (Tab. 1). Thus, under pseudo-static hypothesis: $f_{\max} = 86.96$N. A minimum tension $f_{\min} = 5$N has been imposed on each cable.

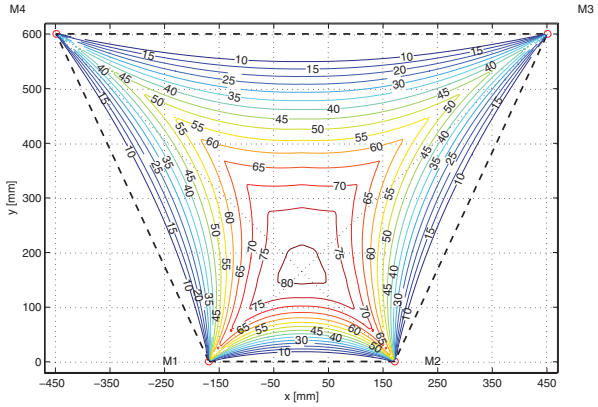

Figure 10. CONTOUR PLOT OF $i_{F,S-4}$[N] FOR SOPHIA-4, WITH $f_{\max} = 87$N AND $f_{\min} = 5$N. THE MAXIMUM ISOTROPIC FORCE IS GREATER THAN 60N INSIDE MOST OF THE WSP.

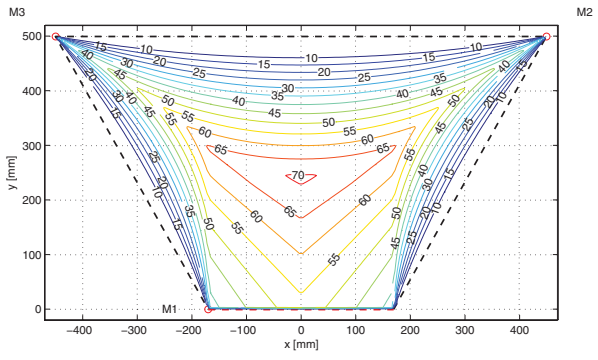

Figure 11. CONTOUR PLOT OF $i_{F,S-3}$[N] FOR SOPHIA-3. THE REDUCED NUMBER OF ACTUATORS YIELDS SMALLER i_F WITH RESPECT TO SOPHIA-4. NONETHELESS, A STATIC FORCE GRATER THAN 50N IS OBTAINED INSIDE MOST OF THE WSP.

Results

Figure 10 and 11 illustrate the contour plots of $i_{F,S-4}$ and $i_{F,S-3}$. Both plots are symmetric, but the reduced number of wires in Sophia-3 results in lower force capabilities: this drawback can be overtaken by mounting more performing motors. If the same statics workspace is analyzed, the most favorable areas are located near the top of the workspace for Sophia-3 and near the bottom of the workspace for Sophia-4. However, the height of the fixed attachment points have been reduced in the former device, so as to draw the favorable region closer to the operator.

The results show that the Cartesian device possesses the best force capabilities, while the SCARA robot has the lowest ones. As compared to the other robots, the wire-based systems present intermediate force performances inside the reference area (Tab. 2); nonetheless, the performance index per unit of perceived mass is much higher than that of the other devices.

		MIT-Manus	Cbm-Motus	Sophia-3	Sophia-4
λ_{max}[kg]	max	2.260	*	0.663	0.718
	min	1.605	*	0.630	0.673
	mean	1.839	2.59	0.646	0.697
	σ	0.162	*	0.008	0.011
$\lambda_{max}/\lambda_{min}$[ ]	max	4.771	*	1.11	1.14
	min	3.328	*	1.00	1.00
	mean	3.844	1	1.05	1.06
	σ	0.357	*	0.03	0.03
i_F [N]	max	*	*	70.76	81.84
	min	*	*	35.50	46.33
	mean	17.86	80	60.44	68.44
	σ	*	*	7.242	7.981

Table 2. PERFORMANCE INDEXES FOR THE ANALYZED PLANAR ROBOTS. A CIRCLE ($r = 140$mm) HAS BEEN USED AS THE REFERENCE WSP TO CALCULATE POSITION-DEPENDENT INDEXES.

CONCLUSION

A comparison between four planar robots for upper-limb rehabilitation was presented. SCARA robots, Cartesian robots and cable-driven robots have been considered and compared in terms of inertial properties and force exertion capabilities. The two cable-driven devices, that are currently being tested in laboratory and will be soon employed in clinical trials with chronic patients, have been presented for the first time. The first of these employs four driven cables to produce a planar force on the end-effector, the second one is based on a three-cable configuration plus a linear actuator to obtain better overall robot performance. The performances of the four robots have been measured in terms of the maximum mass perceived at the end-effector, of the isotropicity of the inertial properties and of the maximum isotropic force over the workspace of each robot.

As a matter of fact, the Cartesian robot proved to have the best isotropicity of the inertial properties, even though this parameter is still very close to unity for cable-driven robots as well. The lowest values of the maximum mass perceived at the end-effector were achieved by cable-driven devices, thanks to the simple and lightweight design that is typical for this kind of robots. These parameters are fundamental as far as the transparency of the device is concerned. Finally, cable-driven systems are comparable to Cartesian robots in terms of maximum isotropic force available in the workspace.

REFERENCES

[1] Truelsena, T., Ekmanb, M., and Boysena, G., 2005. "Cost of stroke in europe". *European Journal of Neurology,* **12**(1), pp. 78–84.

[2] Gresham, G., Duncan, P., and Stason, W., 1995. *Post-stroke rehabilitation. Clinical pratice guideline*, ahcpr pub. 95-0662 ed., Vol. 16. U.S. Dept. of Health Services, Agency for Health Care Policy and Research, Washington, DC.

[3] Rosamond, W., et al., 2007. "Heart disease and stroke statistics-2007 update: A report from the american heart association statistics committee and stroke statistics subcommittee". *Circulation,* **115**, pp. 69–171.

[4] , 2003. Stroke prevention and educational awareness diffusion (spread). the italian guidelines for stroke prevention and treatment. Ed. Hyperphar Group, Milano, Italy.

[5] Campbell, P., 1996. Population projections for states by age, sex, race,and hispanic origin: 1995 to 2025. Tech. Rep. P25-1130, Population Projections Branch, Population Div., Bureau of the Census, Washington, DC, U.S., October.

[6] Butefisch, C., Hummelsheim, H., Denzler, P., and Mauritz, K., May 1995. "Repetitive training of isolated movements improves the outcome of motor rehabilitation of the centrally paretic hand". *Journal of the Neurological Sciences,* **130**(10), pp. 59–68.

[7] Garrett, E. J. P., Milliken, W., and Nudo, R. J., 2000. "Effects of repetitive motor training on movement representations in adult squirrel monkeys: Role of use versus learning". *Neurobiology of Learning and Memory,* **74**.

[8] Harwin, W. S., Patton, J. L., and Edgerton, V. R., 2006. "Challenges and opportunities for robot-mediated neurorehabilitation". *Proceedings of the IEEE*, pp. 1717–1726.

[9] Kwakkel, G., Kollen, B. J., and Krebs, H. I., 2007. "Effects of robot-assisted therapy on upper limb recovery after stroke: A systematic review". *Neurorehabilitation and Neural Repair,* **22**, pp. 111–121.

[10] Reinkensmeyer, D., Galvez, J., Marchal, L., Wolbrecht, E., and Bobrow, J., 13-15 June 2007. "Some key problems for robot-assisted movement therapy research: A perspective

from the university of california at irvine". In Proceedings of the IEEE 10th International Conference on Rehabilitation Robotics, pp. 1009–1015.

[11] Hesse, S., Werner, C., Pohl, M., Rueckriem, S., Mehrhoz, J., and Lingnau, M. L., 2005. "Computerized arm training improves the motor control of the severely affected arm after stoke". *Stroke*, **36**, pp. 1960–1966.

[12] Masiero, S., Celia, A., Rosati, G., and Armani, M., 2007. "Robotic-assisted rehabilitation of the upper limb after acute stroke". *Archives of Physical Medicine and Rehabilitation*, **88**(2), pp. 142–149.

[13] Hogan, N., Krebs, H., Charnnarong, J., Srikrishna, P., and Sharon, A., 1992. "Mit-manus : A workstation for manual therapy and training i". In IEEE International Workshop on Robot and Human Communication, pp. 161–165.

[14] Masia, L., Krebs, H., Cappa, P., and Hogan, N., 2007. "Design and characterization of hand module for whole-arm rehabilitation following stroke". *IEEE/ASME Transaction on Mechatronics*, **12**(4), pp. 399–407.

[15] Casadio, M., Sanguineti, V., Morasso, P., and Arrichiello, V., 2006. "Braccio di ferro: a new haptic workstation for neuromotor rehabilitation.". *Technology Health Care*, **14**(3), pp. 123–142.

[16] Micera, S., et al., 2005. "A simple robotic system for neurorehabilitation". *Autonomous Robots*, **19**(3), pp. 271–284.

[17] Colombo, R., et al., Sept. 2005. "Robotic techniques for upper limb evaluation and rehabilitation of stroke patients". *IEEE transactions on Neural System and Rehabilitation Engineering*, **13**(3), pp. 311–324.

[18] Zollo, L., Accoto, D., Torchiani, F., Formica, D., and Guglielmelli, E., 2008. "Design of a planar robotic machine for neuro-rehabilitation". In Proc. of the IEEE International Conference on Robotics and Automation 2008.

[19] Rosati, G., Gallina, P., and Masiero, S., 2007. "Design, implementation and clinical tests of a wire-based robot for neurorehabilitation". *IEEE Transactions on Neural Systems and Rehabilitation Engineering*, **15**(4), p. 560569.

[20] Rosati, G., Gallina, P., Rossi, A., and Masiero, S., 2006. "Wire-based robots for upper-limb rehabilitation". *International Journal of Assistive Robotics and Mechatronics*, **7**(2), pp. 3–10.

[21] Gallina, P., Rosati, G., and Rossi, A., 2001. "3-d.o.f. wire driven planar haptic interface". *Journal of Int. and Robotic Systems: Theory and Applications*, **32**(1), pp. 23–36.

[22] Dempster, W. T., July 1955. Space requirements of the seated operator, geometrical, kinematic, and mechanical aspects of the body with special reference to the limbs. Tech. rep., Defense Technical Information Center, U.S.

[23] Rosati, G., and Zanotto, D., 2008. "A novel perspective in the design of cable-driven systems". In Proceedings of the 2008 ASME International Mechanical Engineering Congress and Exposition (IMECE).

[24] Yoshikawa, and Tsuneo, 1985. "Manipulability of robotic mechanisms.". *International Journal of Robotics Research*, **4**(2), pp. 3–9.

[25] Krut, S., Company, O., and Pierrot, F., 2004. "Velocity performance indices for parallel mechanisms with actuation redundancy". *Robotica*, **22**(2), pp. 129–139.

[26] Krut, S., Company, O., and Pierrot, F., 2004. "Force performance indexes for parallel mechanisms with actuation redundancy, especially for parallel wire-driven manipulators". In Proc. of the IEEE/RSJ International Conference on Intelligent Robots and Systems (IROS), Vol. 4, pp. 3936–3941.

[27] Asada, H., Mar 1984. "Dynamic analysis and design of robot manipulators using inertia ellipsoids". In Proceedings of the IEEE International Conference on Robotics and Automation, Vol. 1, pp. 94–102.

[28] Khatib, O., 1995. "Inertial properties in robotic manipulation. an object-level framework". *International Journal of Robotics Research*, **14**(1), pp. 19–36.

[29] Yoshikawa, T., 1985. "Dynamic manipulability of robot manipulators.". *Journal of Robotic Systems*, **2**(1), pp. 113–124.

[30] Bowling, A., and Khatib, O., 1995. "Analysis of the acceleration characteristics of non-redundant manipulators". In Proc. of IEEE International Conference on Intelligent Robots and Systems, Vol. 2, pp. 323–328.

[31] Bowling, A., and Khatib, O., 1996. "Optimization of the inertial and acceleration characteristics of manipulators". In Proceedings-IEEE International Conference on Robotics and Automation, Vol. 4, pp. 2883–2889.

[32] Bowling, A., and Khatib, O., 1997. "Design of non-redundant manipulators for optimal dynamic performance". In Proc. of the International Conference on Advanced Robotics, ICAR, pp. 865–872.

[33] Lawrence, D. A., 1993. "Stability and transparency in bilateral teleoperation". *IEEE Transactions on Robotics and Automation*, **9**(5), pp. 624–637.

[34] Bhushan, N., and Shadmehr, R., 1999. "Computational nature of human adaptive control during learning of reaching movements in force fields". *Biological Cybernetics*, **81**(1), pp. 39–60.

[35] Gallina, P., Rossi, A., and Williams II, R. L., 2001. "Planar cable-direct-driven robots, part ii: Dynamics and control". In Proceedings of the ASME Design Engineering Technical Conference, Vol. 2, pp. 1241–1247.

[36] Krebs, H. I., Hogan, N., Aisen, M. L., and Volpe, B. T., 1998. "Robot-aided neurorehabilitation". *IEEE Transactions on Rehabilitation Engineering*, **6**(1), pp. 75–87.